

# Asymptotic-Preserving Neural Networks for Multiscale Kinetic Equations

Shi Jin<sup>1,2</sup>, Zheng Ma<sup>1,2,3</sup>, and Keke Wu<sup>1,\*</sup>

<sup>1</sup> School of Mathematical Sciences, Shanghai Jiao Tong University, Shanghai, 200240, P. R. China.

<sup>2</sup> Institute of Natural Sciences, MOE-LSC, Shanghai Jiao Tong University, Shanghai, 200240, P. R. China.

<sup>3</sup> Qing Yuan Research Institute, Shanghai Jiao Tong University, Shanghai, 200240, China

---

**Abstract.** In this paper, we present two novel Asymptotic-Preserving Neural Networks (APNNs) for tackling multiscale time-dependent kinetic problems, encompassing the linear transport equation and Bhatnagar-Gross-Krook (BGK) equation with diffusive scaling. Our primary objective is to devise efficient and accurate APNN approaches for resolving multiscale kinetic equations. We have established a neural network based on even-odd decomposition and concluded that enforcing the initial condition for the linear transport equation with inflow boundary conditions is crucial. This APNN method based on even-odd parity relaxes the stringent conservation prerequisites while concurrently introducing an auxiliary deep neural network. Additionally, we have incorporated the conservation laws of mass, momentum, and energy for the Boltzmann-BGK equation into the APNN framework by enforcing exact boundary conditions. This is our second contribution. The most notable finding of this study is that approximating the zeroth, first and second moments of the particle density distribution is simpler than the distribution itself. Furthermore, a compelling phenomenon in the training process is that the convergence of density is swifter than that of momentum and energy. Finally, we investigate several benchmark problems to demonstrate the efficacy of our proposed APNN methods.

**AMS subject classifications:** 65N30, 35J66, 41A46, 68T07

**Key words:** Asymptotic-Preserving Neural Networks, even-odd decomposition, conservation laws, multiscale.

---

## 1 Introduction

In scientific modeling, kinetic equations describe the dynamics of particles through a medium with collision and absorption. These equations typically involve multiple spatial and/or temporal scales, as well as nonlocal operators, which present significant

---

\*Corresponding author. *Email addresses:* wukekever@sjtu.edu.cn (K. Wu)

computational challenges in numerical simulations. For a comprehensive overview, please refer to the literature sources [1–4] for a review. Deep learning methods and deep neural networks (DNNs) have garnered immense attention within the scientific community, particularly with respect to resolving partial differential equations (PDEs) [5–12]. To explore alternative machine learning approaches for solving partial differential equations, we suggest that the curious reader consult the exemplary review article [5]. The key motivation behind such methods is to parameterize the solutions or gradients of PDE problems using deep neural networks. These methods ultimately culminate in a minimization problem that is typically high-dimensional and nonconvex. Unlike classical numerical methods, deep learning methods are mesh-free and can solve PDEs in complex domains and geometries. It is also advantageous to possess flexibility and ease of execution, as it opens up the potential to tackle high-dimensional problems. Nonetheless, deep learning methods have several potential drawbacks, including lengthy training times, a lack of convergence, and reduced accuracy. However, the idea of operator learning offers a method to resolve a class of PDEs by training the neural network once [13–18]. It is important to note, however, that a number of issues regarding the convergence theory remain unclear.

In recent years, there has been extensive research conducted on multiscale kinetic equations and hyperbolic systems by employing deep neural networks. This research includes, but is not limited to the works cited in references [19–26]. The kinetic problems, which possess characteristics at multiple scales, have gained significant importance. As we know, there are numerous choices available to build the loss when given a PDE. For instance, variational formulation (DRM), least-squares formulation (PINN, DGM), weak formulation (WAN), etc. Due to the presence of small scales, the vanilla Physics-Informed Neural Networks (PINNs) can be exceedingly unstable for resolving multiscale kinetic equations [21, 22]. A natural question is what kind of loss is “good”. One has to take into consideration conservation, symmetry, parity, etc. Here, an alternative to solving multiscale kinetic equations by utilizing DNNs is to create a loss that can capture the limiting macroscopic behavior (the loss is known as AP), hence justifies the need to use Asymptotic-Preserving Neural Networks (APNNs) [21]. In [21], we proposed an APNN method for time-dependent linear transport equations with diffusive scaling and uncertainties that is based on micro-macro decomposition, and demonstrated that the loss is AP with respect to the Knudsen number that tends to zero.

It is worth noting that the APNN method, based on micro-macro decomposition, imposes rigorous conservation prerequisites. Failure to meet these criteria may result in imprecise outcomes for the ultimate deep neural network approximation. Accordingly, we have progressed towards the refinement of an APNN approach to tackle time-dependent linear transport equations, thereby loosening the stringent prerequisites for conservation. The proposed APNN technique relies on an even-odd decomposition for the time-dependent linear transport equation. The novel loss function exhibits uniform stability in relation to the small Knudsen number, whereby the neural network solution converges uniformly to the macro solution. Noteworthy is the fact that the present

APNN approach is targeted towards the resolution of linear kinetic equations. For the nonlinear Boltzmann-BGK equation, constructing deep neural networks that automatically satisfy the conservation of mass, momentum, and energy akin to APNN based on a micro-macro decomposition poses a formidable challenge. Thus, we have advanced by developing an APNN methodology that unites the fundamental equation with the equation governing local conservation law for the nonlinear Boltzmann-BGK equation.

An outline of this paper is as follows. In Section 2, a detail illustration of Asymptotic-Preserving Neural Networks for linear transport equation and Boltzmann-BGK equation and the construction of loss functions are given. Numerous numerical examples are presented in Section 3 to demonstrate the effectiveness of the APNNs. The paper is concluded in Section 4.

## 2 Methodology

There are three primary components to the DNN framework. The initial component entails utilizing a neural network as an approximation to the solution. The second component involves evaluating the difference between the approximate and exact solutions, which is achieved through population and empirical loss/risk. Finally, the third component is an optimization algorithm that aids in locating a local minimum.

To solve partial differential equations using deep neural networks, the typical procedure is generally analogous:

1. Modeling: define the loss/risk associated to a PDE;
2. Architecture: build a deep neural network (function class) for the trial function;
3. Optimization: minimize the loss over the parameter space.

In terms of proposed APNNs, the primary element entails formulating a loss function that embodies the AP property [21]. The following diagram in Fig. 1 illustrates the idea of APNNs.

First, we introduce the conventional notations for DNNs<sup>†</sup>. An  $L$ -layer feed forward neural network (or fully-connected neural network, FCNet) is defined recursively as,

$$\begin{aligned} f_{\theta}^{[0]}(x) &= x, \\ f_{\theta}^{[l]}(x) &= \sigma \circ (W^{[l-1]} f_{\theta}^{[l-1]}(x) + b^{[l-1]}), 1 \leq l \leq L-1, \\ f_{\theta}(x) &= f_{\theta}^{[L]}(x) = W^{[L-1]} f_{\theta}^{[L-1]}(x) + b^{[L-1]}, \end{aligned} \tag{2.1}$$

where  $W^{[l]} \in \mathbb{R}^{m_{l+1} \times m_l}$ ,  $b^{[l]} \in \mathbb{R}^{m_{l+1}}$ ,  $m_0, m_L$  are the input and output dimension,  $\sigma$  is a scalar function and “ $\circ$ ” means entry-wise operation.

<sup>†</sup>BAAI.2020. Suggested Notation for Machine Learning. <https://github.com/mazhengcn/suggested-notation-for-machine-learning>.

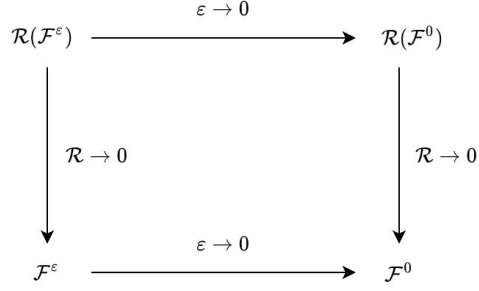


Figure 1: Illustration of APNNs.  $\mathcal{F}^\varepsilon$  is the microscopic equation that depends on the small scale parameter  $\varepsilon$  and  $\mathcal{F}^0$  is its macroscopic limit as  $\varepsilon \rightarrow 0$ , which is independent of  $\varepsilon$ . The latent solution of  $\mathcal{F}^\varepsilon$  is approximated by deep neural networks with its measure denoted by  $\mathcal{R}(\mathcal{F}^\varepsilon)$ . The asymptotic limit of  $\mathcal{R}(\mathcal{F}^\varepsilon)$  as  $\varepsilon \rightarrow 0$ , if exists, is denoted by  $\mathcal{R}(\mathcal{F}^0)$ . If  $\mathcal{R}(\mathcal{F}^0)$  is a good measure of  $\mathcal{F}^0$ , then it is called asymptotic-preserving (AP).

Also, ResNet [27] is composed with several residual blocks with each part containing one input, two weight layers, two activation functions, one identical (shortcut) connection, and one output, which is defined recursively as,

$$\begin{aligned}
f_\theta^{[0]}(x) &= W^{[0]}x + b^{[0]}, \\
f_\theta^{[l]}(x) &= f_\theta^{[l-1]}(x) + \sigma \circ (W_2^{[l-1]} \sigma \circ (W_1^{[l-1]} f_\theta^{[l-1]}(x) + b_1^{[l-1]}) + b_2^{[l-1]}), \quad 1 \leq l \leq L-1, \\
f_\theta(x) &= f_\theta^{[L]}(x) = W^{[L-1]} f_\theta^{[L-1]}(x) + b^{[L-1]},
\end{aligned} \tag{2.2}$$

here we use the same notations as previous for convenience.

We denote the set of parameters by  $\theta$ . For simplicity of neural network presentation, we denote the layers by a list, i.e.,  $[m_0, \dots, m_L]$ . For ResNet, the  $i$ -th block is denoted by  $[m_i, m_i]$  and one can find that  $m_i (i = 1, \dots, L-1)$  is equal.

## 2.1 APNN V2 based on even-odd decomposition

Let us begin by examining the linear transport equation in the context of diffusive scaling, which can be expressed in the following form:

$$\varepsilon \partial_t f + v \partial_x f = \frac{1}{\varepsilon} \left( \frac{1}{2} \int_{-1}^1 f \, dv' - f \right), \quad x_L < x < x_R, \quad -1 \leq v \leq 1, \tag{2.3}$$

with in-flow boundary conditions as

$$\begin{aligned}
f(t, x_L, v) &= F_L(v), \quad \text{for } v > 0, \\
f(t, x_R, v) &= F_R(v), \quad \text{for } v < 0.
\end{aligned} \tag{2.4}$$

Here,  $f(t, x, v)$  is the density distribution of particles at time  $t \in \mathcal{T} := [0, T]$ , space point  $x \in \mathcal{D} := [x_L, x_R] = [0, 1]$ , and traveling in direction  $v \in \Omega := [-1, 1]$ . The parameter  $\varepsilon > 0$  is

the Knudsen number which denotes the ratio of the mean free path over a characteristic length. The initial function is given as a function of  $x$  and  $v$

$$f(0, x, v) = f_0(x, v). \quad (2.5)$$

By splitting equation and define even- and odd-parities as

$$\begin{aligned} r(t, x, v) &= \frac{1}{2}[f(t, x, v) + f(t, x, -v)], 0 \leq v \leq 1, \\ j(t, x, v) &= \frac{1}{2\varepsilon}[f(t, x, v) - f(t, x, -v)], 0 \leq v \leq 1, \end{aligned} \quad (2.6)$$

one can obtain the following system of equations

$$\begin{aligned} \partial_t r + v \partial_x j &= \frac{1}{\varepsilon^2}(\rho - r), \\ \partial_t j + \frac{1}{\varepsilon^2} v \partial_x r &= -\frac{1}{\varepsilon^2} j, \end{aligned} \quad (2.7)$$

where  $\rho = \langle r \rangle := \int_0^1 r(t, x, v) dv$ .

Thus far, we have implemented the even-odd system, but simply employing neural networks for  $r$  and  $j$  does not result in an APNN framework. In order to establish an APNN framework, our next step involves the introduction of  $\rho$  as a mediator between  $r$  and  $j$  within this system.

By integrating over  $v$ , the first equation gives

$$\partial_t \langle r \rangle + \int_0^1 v \partial_x j dv = \frac{1}{\varepsilon^2}(\rho - \langle r \rangle), \quad (2.8)$$

and since  $\rho = \langle r \rangle$  one can write as follows

$$\partial_t \rho + \int_0^1 v \partial_x j dv = 0. \quad (2.9)$$

Finally, Eq. (2.7) and Eq. (2.9) together with the constraint  $\rho = \langle r \rangle$  constitute the even-odd formulation of Eq. (2.3):

$$\begin{cases} \varepsilon^2 \partial_t r + \varepsilon^2 v \partial_x j = \rho - r, \\ \varepsilon^2 \partial_t j + v \partial_x r = -j, \\ \partial_t \rho + \langle v \partial_x j \rangle = 0, \\ \rho = \langle r \rangle. \end{cases} \quad (2.10)$$

When  $\varepsilon \rightarrow 0$ , the above equation formally approaches

$$\begin{cases} r = \rho, \\ j = -v \partial_x r, \\ \partial_t \rho + \langle v \partial_x j \rangle = 0. \end{cases} \quad (2.11)$$

Substituting the first equation into the second equation gives  $j = -v\partial_x\rho$  and plugging into the third equation will result

$$\partial_t\rho - \frac{1}{3}\partial_{xx}\rho = 0, \quad (2.12)$$

which is exactly the diffusion equation.

**Remark 1.** In Eq. (2.10) we singled out the equation of local conservation law  $\partial_t\rho + \langle v\partial_x j \rangle = 0$  is necessary in constructing the APNN loss. By coupling these equations of  $r, j$  and  $\rho$ , one can obtain the loss for the diffusion limit equation.

For solving the linear transport equation by deep neural networks, we need to use DNNs to parametrize three functions  $\rho(t, x), r(t, x, v)$  and  $j(t, x, v)$ . So here three networks are used. First,

$$\rho_\theta^{\text{NN}}(t, x) := \exp\left(-\tilde{\rho}_\theta^{\text{NN}}(t, x)\right) \approx \rho(t, x), \quad (2.13)$$

Second,

$$r_\theta^{\text{NN}}(t, x, v) := \exp\left(-\frac{1}{2}(\tilde{r}_\theta^{\text{NN}}(t, x, v) + \tilde{r}_\theta^{\text{NN}}(t, x, -v))\right) \approx r(t, x, v), \quad (2.14)$$

and

$$j_\theta^{\text{NN}}(t, x, v) := \tilde{j}_\theta^{\text{NN}}(t, x, v) - \tilde{j}_\theta^{\text{NN}}(t, x, -v) \approx j(t, x, v), \quad (2.15)$$

which automatically satisfy the even-odd properties.

Then we propose the least square of the residual of the even-odd system as the APNN loss

$$\mathcal{R}_{\text{APNN}}^\varepsilon = \mathcal{R}_{\text{residual}}^\varepsilon + \mathcal{R}_{\text{constraint}}^\varepsilon + \mathcal{R}_{\text{initial}}^\varepsilon + \mathcal{R}_{\text{boundary}}^\varepsilon, \quad (2.16)$$

where  $\mathcal{R}_{\text{residual}}^\varepsilon, \mathcal{R}_{\text{APNN, constraint}}^\varepsilon, \mathcal{R}_{\text{APNN, boundary}}^\varepsilon, \mathcal{R}_{\text{APNN, initial}}^\varepsilon$  are denoted by

$$\begin{aligned} \mathcal{R}_{\text{residual}}^\varepsilon &= \frac{\lambda_1}{|\mathcal{T} \times \mathcal{D} \times \Omega|} \int_{\mathcal{T}} \int_{\mathcal{D}} \int_{\Omega} |\varepsilon^2 \partial_t r_\theta^{\text{NN}} + \varepsilon^2 v \partial_x j_\theta^{\text{NN}} - (\rho_\theta^{\text{NN}} - r_\theta^{\text{NN}})|^2 dv dx dt \\ &\quad + \frac{\lambda_2}{|\mathcal{T} \times \mathcal{D} \times \Omega|} \int_{\mathcal{T}} \int_{\mathcal{D}} \int_{\Omega} |\varepsilon^2 \partial_t j_\theta^{\text{NN}} + v \partial_x r_\theta^{\text{NN}} - (-j_\theta^{\text{NN}})|^2 dv dx dt \\ &\quad + \frac{\lambda_3}{|\mathcal{T} \times \mathcal{D}|} \int_{\mathcal{T}} \int_{\mathcal{D}} |\partial_t \rho_\theta^{\text{NN}} + \langle v \partial_x j_\theta^{\text{NN}} \rangle|^2 dx dt, \\ \mathcal{R}_{\text{constraint}}^\varepsilon &= \frac{\lambda_4}{|\mathcal{T} \times \mathcal{D}|} \int_{\mathcal{T}} \int_{\mathcal{D}} |\rho_\theta^{\text{NN}} - \langle r_\theta^{\text{NN}} \rangle|^2 dx dt, \\ \mathcal{R}_{\text{initial}}^\varepsilon &= \frac{\lambda_5}{|\mathcal{D}|} \int_{\mathcal{D}} |\rho_\theta^{\text{NN}}(0, x) - \langle f_0 \rangle|^2 dx + \frac{\lambda_6}{|\mathcal{D} \times \Omega|} \int_{\mathcal{D}} \int_{\Omega} |\mathcal{I}(r_\theta^{\text{NN}} + \varepsilon j_\theta^{\text{NN}}) - f_0|^2 dv dx, \\ \mathcal{R}_{\text{boundary}}^\varepsilon &= \frac{\lambda_7}{|\mathcal{T} \times \partial \mathcal{D} \times \Omega|} \int_{\mathcal{T}} \int_{\partial \mathcal{D}} \int_{\Omega} |\mathcal{B}(r_\theta^{\text{NN}} + \varepsilon j_\theta^{\text{NN}}) - F_B|^2 dv dx dt. \end{aligned} \quad (2.17)$$

Here,  $\lambda_i$  ( $i=1,2,\dots,7$ ) are the penalty weights to be tuned and  $|\mathcal{X}|$  denotes the measure of the domain  $\mathcal{X}$ . Besides,  $\mathcal{I}, \mathcal{B}$  are the initial and boundary operators.

Now the AP property of this loss can be carried out by considering its behavior for  $\varepsilon$  small. One may only need to focus on the first three terms of Eq. (2.17)

$$\begin{aligned} \mathcal{R}_{\text{APNN, residual}}^\varepsilon &= \frac{\lambda_1}{|\mathcal{T} \times \mathcal{D} \times \Omega|} \int_{\mathcal{T}} \int_{\mathcal{D}} \int_{\Omega} |\varepsilon^2 \partial_t r_\theta^{\text{NN}} + \varepsilon^2 v \partial_x j_\theta^{\text{NN}} - (\rho_\theta^{\text{NN}} - r_\theta^{\text{NN}})|^2 dv dx dt \\ &\quad + \frac{\lambda_2}{|\mathcal{T} \times \mathcal{D} \times \Omega|} \int_{\mathcal{T}} \int_{\mathcal{D}} \int_{\Omega} |\varepsilon^2 \partial_t j_\theta^{\text{NN}} + v \partial_x r_\theta^{\text{NN}} - (-j_\theta^{\text{NN}})|^2 dv dx dt \\ &\quad + \frac{\lambda_3}{|\mathcal{T} \times \mathcal{D}|} \int_{\mathcal{T}} \int_{\mathcal{D}} |\partial_t \rho_\theta^{\text{NN}} + \langle v \partial_x j_\theta^{\text{NN}} \rangle|^2 dx dt. \end{aligned} \quad (2.18)$$

Sending  $\varepsilon \rightarrow 0$ , this will naturally lead to

$$\begin{aligned} \mathcal{R}_{\text{APNN, residual}}^0 &= \frac{\lambda_1}{|\mathcal{T} \times \mathcal{D} \times \Omega|} \int_{\mathcal{T}} \int_{\mathcal{D}} \int_{\Omega} |\rho_\theta^{\text{NN}} - r_\theta^{\text{NN}}|^2 dv dx dt \\ &\quad + \frac{\lambda_2}{|\mathcal{T} \times \mathcal{D} \times \Omega|} \int_{\mathcal{T}} \int_{\mathcal{D}} \int_{\Omega} |v \partial_x r_\theta^{\text{NN}} - (-j_\theta^{\text{NN}})|^2 dv dx dt \\ &\quad + \frac{\lambda_3}{|\mathcal{T} \times \mathcal{D}|} \int_{\mathcal{T}} \int_{\mathcal{D}} |\partial_t \rho_\theta^{\text{NN}} + \langle v \partial_x j_\theta^{\text{NN}} \rangle|^2 dx dt, \end{aligned} \quad (2.19)$$

which is the least square loss of Eq. (2.11)

$$\begin{cases} r = \rho, \\ j = -v \partial_x r, \\ \partial_t \rho + \langle v \partial_x j \rangle = 0. \end{cases} \quad (2.20)$$

Same as previous derivation the third equation yields the diffusion Eq. (2.12). Thus this proposed method is an APNN method.

## 2.2 APNN for Boltzmann-BGK equation

Boltzmann equation is the well-known kinetic model which captures the evolution of density distribution for rarefied gases [28, 29]. The  $d_x$ -dimensional Boltzmann equation can be expressed in a dimensionless form as

$$\partial_t f + v \cdot \nabla_x f = \frac{1}{\varepsilon} \mathcal{C}(f, f), \quad t > 0, \quad (x, v) \in \mathbb{R}^{d_x} \times \mathbb{R}^{d_v}, \quad (2.21)$$

where the function, denoted by  $f(t, x, v)$ , characterizes the velocity distribution of particles, while the right-hand side of the equation  $\frac{1}{\varepsilon} \mathcal{C}(f, f)$  represents the term associated with collisions among particles and is a non-linear operator. Its action is generally limited to the velocity-dependent behavior of  $f$  exclusively. The parameter  $\varepsilon > 0$  is the Knudsen number which denotes the ratio of the mean free path over a characteristic length.

The so-called Boltzmann collision operator  $\mathcal{C}(f, f)$  possesses fundamental physical properties [30] as

1. conservation of mass, momentum and energy

$$\int_{\mathbb{R}^{d_v}} m\mathcal{C}(f, f)dv = 0, m = \left(1, v, \frac{1}{2}|v|^2\right)^T.$$

2. The entropy dissipation inequality

$$\int_{\mathbb{R}^{d_v}} \mathcal{C}(f, f) \cdot \log(f)dv \leq 0.$$

3. The non-negative equilibrium functions  $f$ , namely those satisfying  $\mathcal{C}(f, f) = 0$ , correspond to the local Maxwellian distributions defined by

$$M(U) = \frac{\rho}{(2\pi T)^{\frac{d_v}{2}}} \exp\left(-\frac{|v-u|^2}{2T}\right), \quad (2.22)$$

where density  $\rho(t, x)$ , macroscopic velocity  $u(t, x)$  and temperature  $T(t, x)$  of the gas are the continuum description by field variables defined by

$$\begin{aligned} \rho &= \int_{\mathbb{R}^{d_v}} f(v)dv = \int_{\mathbb{R}^{d_v}} M(U)dv, \\ u &= \frac{1}{\rho} \int_{\mathbb{R}^{d_v}} v f(v)dv = \frac{1}{\rho} \int_{\mathbb{R}^{d_v}} v M(U)dv, \\ T &= \frac{1}{\rho} \int_{\mathbb{R}^{d_v}} |u-v|^2 f(v)dv = \frac{1}{\rho} \int_{\mathbb{R}^{d_v}} |u-v|^2 M(U)dv. \end{aligned}$$

Here,  $U$  is the hydrodynamic variables (density, momentum and energy) which is a vector of the moments of  $f$ :

$$U = \left(\rho, \rho u, \frac{1}{2}\rho|u|^2 + \frac{1}{2}\rho T\right)^T = \int_{\mathbb{R}^{d_v}} m f dv, \quad (2.23)$$

and density  $\rho(t, x)$ , macroscopic velocity  $u(t, x)$  and temperature  $T(t, x)$  are the continuum description by field variables.

As the frequency of collisions increases significantly, the mean free path, i.e., the distance a particle covers between two consecutive collisions, becomes comparatively smaller than a characteristic length of the physical domain under consideration. In such a scenario, a macroscopic portrayal of the gas seems more suitable. The compressible Euler and compressible Navier-Stokes (CNS) equations serve as primary instances, as they elucidate the development of averaged quantities like the local density, momentum, and energy of the gas. The CNS model surpasses the Euler equations in terms of accuracy, owing to its inclusion of factors such as viscosity and heat conductivity, which results in a correction of order  $\varepsilon$ . Physically, classical fluid models may not fully



capture the macroscopic evolution of gas, particularly when it is in a far from equilibrium state. Fluid models, such as the compressible Euler or CNS type, are classically derived by using the moment method in conjunction with perturbation techniques like the Hilbert or Chapman-Enskog expansions [29]. Specifically, the derivation of the CNS model from the Boltzmann equation in the fluid regime provides an approximation of viscosity and heat fluxes in the gas, up to the order of  $\varepsilon^2$ . The primary challenge of solving Boltzmann equation stems from the fact that the aforementioned term  $\frac{1}{\varepsilon}$  stiffens as  $\varepsilon$  approaches zero, thereby entering a fluid regime. When considering this scenario, the resolution of the Boltzmann equation through a conventional explicit numerical method necessitates a time step of  $\varepsilon$  magnitude. This results in computationally costly operations when  $\varepsilon$  is small.

At the level of Euler asymptotics, numerous authors have suggested asymptotically preserving numerical approximations to solve the Boltzmann equation. For instance, numerical methods that are capable of capturing the accurate Euler limit have been proposed in [31], specifically in the context of the Bhatnagar-Gross-Krook (BGK) equation [32].

The intricate nature of the Boltzmann collision operator is circumvented by considering the more streamlined BGK model in our study as follows

$$\partial_t f + v \cdot \nabla_x f = \frac{1}{\varepsilon} (M(U) - f), \quad v \in \mathbb{R}, \quad (2.24)$$

here  $f(t, x, v)$  is the density distribution of particles at time  $t \in \mathcal{T} := [0, T]$ , space point  $x \in \mathcal{D} := [x_L, x_R] = [-0.5, 0.5]$ , and traveling in direction  $v \in \mathbb{R}$ ,  $M(U)$  denotes the local Maxwellian distribution function. Notice that the Boltzmann-BGK equation is an integro-differential equation with its nonlinear and non-local collision operator. One can easily check that BGK operator satisfies mass, momentum and energy conservation.

Due to the properties of conserving mass, momentum and energy of collision operator, one can multiply the BGK equation Eq. (2.24) by  $m(v)$  and then integrate them with respect to  $v$  to obtain the following equations:

$$\partial_t \langle mf \rangle + \nabla_x \cdot \langle vmf \rangle = 0, \text{ where } \langle g \rangle = \int_{\mathbb{R}} g(v) dv, \quad (2.25)$$

i.e.,

$$\partial_t \begin{pmatrix} \rho \\ \rho u \\ \frac{1}{2} \rho |u|^2 + \frac{1}{2} \rho T \end{pmatrix} + \nabla_x \cdot \langle vmf \rangle = 0. \quad (2.26)$$

Finally, Eq. (2.24) and Eq. (2.26) with the constrain Eq. (2.23) constitute the systems of BGK model:

$$\begin{cases} \varepsilon (\partial_t f + v \partial_x f) = M(U) - f, \\ \partial_t U + \nabla_x \cdot \langle vmf \rangle = 0, \\ U = \langle mf \rangle. \end{cases} \quad (2.27)$$

While considering the Boltzmann-BGK equation, similar to APNN v1 [21], it is crucial to highlight that our observation indicates the difficulty in creating a neural network for the non-equilibrium that adequately maintains the simultaneous conservation of mass, momentum and energy, despite its micro-macro decomposition technique for resolution [30]. Thus, inspired by the Gas-Kinetic scheme [33,34], we incorporated the original equation concerning function  $f$  into the system of local conservation laws Eq. (2.25) or Eq. (2.26), thereby closing the newly established system of equations.

For brevity we use the notation  $W(t,x) = (\rho(t,x), u(t,x), T(t,x))^T$ . The boundary conditions for the variables  $\rho, u, T$  in our study are defined as

$$\begin{aligned}\rho(t, x_L) &= \rho_L, \rho(t, x_R) = \rho_R, \\ u(t, x_L) &= u_L = 0, u(t, x_R) = u_R = 0, \\ T(t, x_L) &= T_L, T(t, x_R) = T_R,\end{aligned}$$

i.e.,

$$W_L = (\rho_L, u_L, T_L)^T, W_R = (\rho_R, u_R, T_R)^T.$$

The initial condition of  $f$  is computed by the initial functions  $W_0(x) = (\rho_0(x), u_0(x), T_0(x))^T$ :

$$f(0, x, v) = \frac{\rho_0}{(2\pi T_0)^{\frac{1}{2}}} \exp\left(-\frac{|v - u_0|^2}{2T_0}\right) := f_0(x, v).$$

Here we restrict the range of velocity  $\mathbb{R}$  to a bounded symmetrical domain  $\Omega = [-V, V]$  with  $V = 10$  and this assumption might be realistic in many studies.

First we need to use DNNs to parametrize four functions  $f(t, x, v), \rho(t, x), u(t, x)$  and  $T(t, x)$ . So here four networks are used. The time and velocity variable  $t, v$  are normalized into  $[0, 1]$  and  $[-1, 1]$  with scaling  $\bar{t} = t/T, \bar{v} = v/V$ . It is worth pointing out that this normalization is necessary to alleviate the mismatching of the range of temporal domain and velocity domain. One can construct four DNNs as follows:

$$f_{\theta}^{\text{NN}}(t, x, v) := \ln\left(1 + \exp(\tilde{f}_{\theta}^{\text{NN}}(\bar{t}, x, \bar{v}))\right) > 0, \quad (2.28)$$

and

$$\begin{aligned}\rho_{\theta}^{\text{NN}}(t, x) &:= \rho_L^{\frac{x_R - x}{x_R - x_L}} \cdot \rho_R^{\frac{x - x_L}{x_R - x_L}} \cdot \exp\left((x - x_L)(x_R - x) \cdot \tilde{\rho}_{\theta}^{\text{NN}}(\bar{t}, x)\right) > 0, \\ u_{\theta}^{\text{NN}}(t, x) &:= \sqrt{(x - x_L)(x_R - x)} \cdot \tilde{u}_{\theta}^{\text{NN}}(\bar{t}, x), \\ T_{\theta}^{\text{NN}}(t, x) &:= T_L^{\frac{x_R - x}{x_R - x_L}} \cdot T_R^{\frac{x - x_L}{x_R - x_L}} \cdot \exp\left((x - x_L)(x_R - x) \cdot \tilde{T}_{\theta}^{\text{NN}}(\bar{t}, x)\right) > 0,\end{aligned} \quad (2.29)$$

which  $\rho_{\theta}^{\text{NN}}, u_{\theta}^{\text{NN}}, T_{\theta}^{\text{NN}}$  automatically satisfy the boundary conditions. In this problem, to keep  $f$  positive,  $\ln(1 + \exp(\cdot))$  is applied for constructing  $f_{\theta}^{\text{NN}}$ . The advantage of this structure lies in the parity of magnitudes between  $f_{\theta}^{\text{NN}}$  and  $\tilde{f}_{\theta}^{\text{NN}}$  when their magnitude exceeds a certain threshold.

Then we propose the least square of the residual of BGK model as the APNN loss

$$\mathcal{R}_{\text{APNN}}^\varepsilon = \mathcal{R}_{\text{residual}}^\varepsilon + \mathcal{R}_{\text{claw}}^\varepsilon + \mathcal{R}_{\text{constraint}}^\varepsilon + \mathcal{R}_{\text{boundary}}^\varepsilon + \mathcal{R}_{\text{initial}}^\varepsilon, \quad (2.30)$$

where  $\mathcal{R}_{\text{residual}}^\varepsilon, \mathcal{R}_{\text{claw}}^\varepsilon, \mathcal{R}_{\text{constraint}}^\varepsilon, \mathcal{R}_{\text{boundary}}^\varepsilon, \mathcal{R}_{\text{initial}}^\varepsilon$  are denoted by

$$\begin{aligned} \mathcal{R}_{\text{APNN, residual}}^\varepsilon &= \frac{\lambda_1}{|\mathcal{T} \times \mathcal{D} \times \Omega|} \int_{\mathcal{T}} \int_{\mathcal{D}} \int_{\Omega} |\varepsilon(\partial_t f_\theta^{\text{NN}} + v \nabla_x f_\theta^{\text{NN}}) - (M(U_\theta^{\text{NN}}) - f_\theta^{\text{NN}})|^2 dv dx dt, \\ \mathcal{R}_{\text{APNN, claw}}^\varepsilon &= \frac{\lambda_2}{|\mathcal{T} \times \mathcal{D}|} \cdot \int_{\mathcal{T}} \int_{\mathcal{D}} |\partial_t U_\theta^{\text{NN}} + \nabla_x \langle v m f_\theta^{\text{NN}} \rangle|^2 dx dt, \\ \mathcal{R}_{\text{APNN, constraint}}^\varepsilon &= \frac{\lambda_3}{|\mathcal{T} \times \mathcal{D}|} \cdot \int_{\mathcal{T}} \int_{\mathcal{D}} |U_\theta^{\text{NN}} - \langle m f_\theta^{\text{NN}} \rangle|^2 dx dt, \\ \mathcal{R}_{\text{APNN, boundary}}^\varepsilon &= \frac{\lambda_4}{|\mathcal{T}|} \int_{\mathcal{T}} |W_\theta^{\text{NN}}(t, x_L) - W_L|^2 + |W_\theta^{\text{NN}}(t, x_R) - W_R|^2 dt, \\ \mathcal{R}_{\text{APNN, initial}}^\varepsilon &= \frac{\lambda_5}{|\mathcal{D}|} \int_{\mathcal{D}} |W_\theta^{\text{NN}}(0, x) - W_0(x)|^2 dx + \frac{\lambda_6}{|\mathcal{D} \times \Omega|} \int_{\mathcal{D}} \int_{\Omega} |f_\theta^{\text{NN}}(0, x, v) - f_0(x, v)|^2 dv dx, \end{aligned} \quad (2.31)$$

and  $U_\theta^{\text{NN}}, W_\theta^{\text{NN}}$  are computed by  $\rho_\theta^{\text{NN}}, u_\theta^{\text{NN}}$  and  $T_\theta^{\text{NN}}$ .

The AP property of this loss can now be realized by examining its behavior for infinitesimally small values of  $\varepsilon$ . One may only need to focus on the first two terms of Eq. (2.30)

$$\mathcal{R}_{\text{APNN}}^\varepsilon = \mathcal{R}_{\text{residual}}^\varepsilon + \mathcal{R}_{\text{claw}}^\varepsilon, \quad (2.32)$$

$$\begin{aligned} \mathcal{R}_{\text{APNN, residual}}^\varepsilon &= \frac{\lambda_1}{|\mathcal{T} \times \mathcal{D} \times \Omega|} \int_{\mathcal{T}} \int_{\mathcal{D}} \int_{\Omega} |\varepsilon(\partial_t f_\theta^{\text{NN}} + v \nabla_x f_\theta^{\text{NN}}) - (M(U_\theta^{\text{NN}}) - f_\theta^{\text{NN}})|^2 dv dx dt, \\ \mathcal{R}_{\text{APNN, claw}}^\varepsilon &= \frac{\lambda_2}{|\mathcal{T} \times \mathcal{D}|} \cdot \int_{\mathcal{T}} \int_{\mathcal{D}} |\partial_t U_\theta^{\text{NN}} + \nabla_x \langle v m f_\theta^{\text{NN}} \rangle|^2 dx dt. \end{aligned} \quad (2.33)$$

Sending  $\varepsilon \rightarrow 0$ , this will naturally lead to

$$\begin{aligned} \mathcal{R}_{\text{APNN, residual}}^\varepsilon &= \frac{\lambda_1}{|\mathcal{T} \times \mathcal{D} \times \Omega|} \int_{\mathcal{T}} \int_{\mathcal{D}} \int_{\Omega} |M(U_\theta^{\text{NN}}) - f_\theta^{\text{NN}}|^2 dv dx dt, \\ \mathcal{R}_{\text{APNN, claw}}^\varepsilon &= \frac{\lambda_2}{|\mathcal{T} \times \mathcal{D}|} \cdot \int_{\mathcal{T}} \int_{\mathcal{D}} |\partial_t U_\theta^{\text{NN}} + \nabla_x \langle v m f_\theta^{\text{NN}} \rangle|^2 dx dt, \end{aligned} \quad (2.34)$$

which is the least square loss of fluid dynamics equations. Thus, we have check that this loss is AP by sending  $\varepsilon \rightarrow 0$ . Finally we put a schematic plot of our APNN method for Boltzmann-BGK problem in Fig. 2.

### 3 Numerical results

In this section, some numerical experiments have been carried out to verify the performance of our proposed APNN methods. Since the operator of  $v$  in the loss of APNNs are integrals, we approximate them with Gauss-Legendre quadrature rule.

The reference solutions are obtained by standard finite difference method and we will check the relative  $\ell^2$  error of the solution  $s(x)(\rho, u, T)$  of APNN method, e.g. for 1d case,

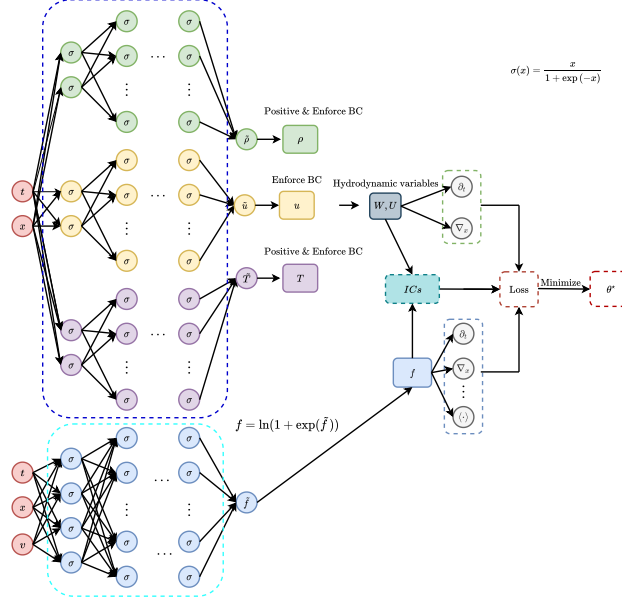


Figure 2: Schematic of APNNs for solving the Boltzmann-BGK equation.

$$\text{error} := \sqrt{\frac{\sum_j |s_{\theta,j}^{\text{NN}} - s_j^{\text{ref}}|^2}{\sum_j |s_j^{\text{ref}}|^2}}. \quad (3.1)$$

### 3.1 Experiment setting

The activation function we used is  $\sigma(x) = \tanh(x)$  for linear transport problems and  $\sigma(x) = x/(1 + \exp(-x))$  for BGK problems. More specifically, fully-connected neural network is applied for the linear transport problem while ResNet is used for the BGK problem for better performance. The number of quadrature points is 30 for linear transport equation and 64 for Boltzmann-BGK equation. To train the networks, the Adam [35] version of the gradient descent methods is used to solve the optimization problem with Xavier initialization. In practice of these cases, we need to tune the hyperparameters, such as neural network architecture, learning rate, batch size and so on, to obtain a good level of accuracy [36]. As a matter of experience one may tune the weights of loss terms to make them at the same level and a decreasing annealing schedule for learning rate is used for better numerical performance. We use an exponential

decay with a decay rate of 0.96 and a decay step of 200 iterations.

The APNN empirical risk for the even-odd system of linear transport equation is

$$\mathcal{R}_{\text{APNN, transport}}^\varepsilon = \mathcal{R}_{\text{residual}}^\varepsilon + \mathcal{R}_{\text{constraint}}^\varepsilon + \mathcal{R}_{\text{initial}}^\varepsilon + \mathcal{R}_{\text{boundary}}^\varepsilon, \quad (3.2)$$

where  $\mathcal{R}_{\text{residual}}^\varepsilon, \mathcal{R}_{\text{constraint}}^\varepsilon, \mathcal{R}_{\text{boundary}}^\varepsilon, \mathcal{R}_{\text{initial}}^\varepsilon$  are denoted by

$$\begin{aligned} \mathcal{R}_{\text{residual}}^\varepsilon &= \frac{\lambda_1}{N_1^{(1)}} \sum_{i=1}^{N_1^{(1)}} |\varepsilon^2 \partial_t r_\theta^{\text{NN}}(t_i, x_i, v_i) + \varepsilon^2 v \partial_x j_\theta^{\text{NN}}(t_i, x_i, v_i) \\ &\quad - (\rho_\theta^{\text{NN}}(t_i, x_i) - r_\theta^{\text{NN}}(t_i, x_i, v_i))|^2 \\ &\quad + \frac{\lambda_2}{N_1^{(2)}} \sum_{i=1}^{N_1^{(2)}} |\varepsilon^2 \partial_t j_\theta^{\text{NN}}(t_i, x_i, v_i) + v \partial_x r_\theta^{\text{NN}}(t_i, x_i, v_i) - (-j_\theta^{\text{NN}}(t_i, x_i, v_i))|^2 \\ &\quad + \frac{\lambda_3}{N_1^{(3)}} \sum_{i=1}^{N_1^{(3)}} |\partial_t \rho_\theta^{\text{NN}}(t_i, x_i) + \langle v \partial_x j_\theta^{\text{NN}} \rangle(t_i, x_i)|^2, \\ \mathcal{R}_{\text{constraint}}^\varepsilon &= \frac{\lambda_4}{N_2} \sum_{i=1}^{N_2} |\rho_\theta^{\text{NN}}(t_i, x_i) - \langle r_\theta^{\text{NN}} \rangle(t_i, x_i)|^2, \\ \mathcal{R}_{\text{initial}}^\varepsilon &= \frac{\lambda_5}{N_3} \sum_{i=1}^{N_3} |\rho_\theta^{\text{NN}}(0, x_i) - \langle f_0 \rangle(x_i)|^2 + \frac{\lambda_6}{N_4} \sum_{i=1}^{N_4} |\mathcal{I}(r_\theta^{\text{NN}} + \varepsilon j_\theta^{\text{NN}})(x_i, v_i) - f_0(x_i, v_i)|^2, \\ \mathcal{R}_{\text{boundary}}^\varepsilon &= \frac{\lambda_7}{N_5} \sum_{i=1}^{N_5} |\mathcal{B}(r_\theta^{\text{NN}} + \varepsilon j_\theta^{\text{NN}})(t_i, x_i, v_i) - F_B(t_i, x_i, v_i)|^2. \end{aligned} \quad (3.3)$$

Here,  $N_1^{(1)}, N_1^{(2)}, N_1^{(3)}, N_2, N_3, N_4, N_5$  are the number of sample points of domains  $|\mathcal{T} \times \mathcal{D} \times \Omega|, |\mathcal{T} \times \mathcal{D} \times \Omega|, |\mathcal{T} \times \mathcal{D}|, |\mathcal{T} \times \mathcal{D}|, |\mathcal{D}|, |\mathcal{D} \times \Omega|, |\mathcal{T} \times \partial \mathcal{D} \times \Omega|$ .

The APNN empirical risk for the system of Boltzmann-BGK equation is

$$\mathcal{R}_{\text{APNN, BGK}}^\varepsilon = \mathcal{R}_{\text{residual}}^\varepsilon + \mathcal{R}_{\text{constraint}}^\varepsilon + \mathcal{R}_{\text{boundary}}^\varepsilon + \mathcal{R}_{\text{initial}}^\varepsilon, \quad (3.4)$$

where  $\mathcal{R}_{\text{residual}}^\varepsilon, \mathcal{R}_{\text{claw}}^\varepsilon, \mathcal{R}_{\text{constraint}}^\varepsilon, \mathcal{R}_{\text{boundary}}^\varepsilon, \mathcal{R}_{\text{initial}}^\varepsilon$  are denoted by

$$\begin{aligned} \mathcal{R}_{\text{residual}}^\varepsilon &= \frac{\lambda_1}{N_1} \sum_{i=1}^{N_1} |\varepsilon(\partial_t f_\theta^{\text{NN}}(t_i, x_i, v_i) + v \nabla_x f_\theta^{\text{NN}}(t_i, x_i, v_i)) - (M(U_\theta^{\text{NN}}) - f_\theta^{\text{NN}})(t_i, x_i, v_i)|^2, \\ \mathcal{R}_{\text{claw}}^\varepsilon &= \frac{\lambda_2}{N_2} \sum_{i=1}^{N_2} |\partial_t U_\theta^{\text{NN}}(t_i, x_i) + \nabla_x \langle v m f_\theta^{\text{NN}} \rangle(t_i, x_i)|^2, \\ \mathcal{R}_{\text{constraint}}^\varepsilon &= \frac{\lambda_3}{N_3} \sum_{i=1}^{N_3} |U_\theta^{\text{NN}}(t_i, x_i) - \langle m f_\theta^{\text{NN}} \rangle(t_i, x_i)|^2, \\ \mathcal{R}_{\text{boundary}}^\varepsilon &= \frac{\lambda_4}{N_4} \sum_{i=1}^{N_4} |W_\theta^{\text{NN}}(t_i, x_L) - W_L|^2 + |W_\theta^{\text{NN}}(t_i, x_R) - W_R|^2, \\ \mathcal{R}_{\text{initial}}^\varepsilon &= \frac{\lambda_5}{N_5} \sum_{i=1}^{N_5} |W_\theta^{\text{NN}}(0, x_i) - W_0(x_i)|^2 + \frac{\lambda_6}{N_6} \sum_{i=1}^{N_6} |f_\theta^{\text{NN}}(0, x_i, v_i) - f_0(x_i, v_i)|^2. \end{aligned} \quad (3.5)$$

Here,  $N_i (i=1, \dots, 6)$  is the number of sample points of corresponding domain.

### 3.2 Problem 1: APNNs for solving linear transport equations

Consider the linear transport equation:

$$\varepsilon \partial_t f + v \partial_x f = \frac{1}{\varepsilon} \left( \frac{1}{2} \int_{-1}^1 f \, dv' - f \right),$$

and recall that the even-odd system of linear transport equation is

$$\begin{cases} \varepsilon^2 \partial_t r + \varepsilon^2 v \partial_x j = \rho - r, \\ \varepsilon^2 \partial_t j + v \partial_x r = -j, \\ \partial_t \rho + \langle v \partial_x j \rangle = 0, \\ \rho = \langle r \rangle. \end{cases}$$

Case I and II are studied for problem 1 with constant scattering coefficient 1 for  $\varepsilon = 10^{-3}, 10^{-8}$ . Furthermore, we focus on an uncertainty quantification problem for  $\varepsilon = 10^{-5}$  in Case III.

#### Case I. Inflow condition with $\varepsilon = 10^{-3}$

Let  $\varepsilon = 10^{-3}$ , in-flow boundary condition be  $F_L(v) = 1, F_R(v) = 0$ , and initial condition be  $f_0(x, v) = 0$ . Note that the function  $f$  exhibits a discontinuity at  $t = 0$  due to the conditions  $F_L(v) = 1, F_R(v) = 0$ , and  $f_0(x, v) = 0$ . To enhance numerical performance,  $\rho_\theta^{\text{NN}}$  can be further designed to inherently satisfy the initial condition.:

$$\rho_\theta^{\text{NN}}(t, x) := t \cdot \exp\left(-\tilde{\rho}_\theta^{\text{NN}}(t, x)\right) \approx \rho(t, x). \quad (3.6)$$

Fig. 3 depicts the estimated density, denoted as  $\rho$ , using APNNs in comparison to the reference solution at time instances  $t=0, 0.05, 0.1$ . It is evident that the approximated solutions exhibit favorable accuracy at both  $t=0, 0.05$  and  $t=0.1$ .

The numerical performance of enforcing the initial condition and the soft constraint  $\rho = \langle r \rangle$  is deliberated as follows. The ensuing phenomena have been observed in all the experiments we have conducted.

Fig. 4 illustrates the performance resulting from the imprecise enforcement of the initial condition. Owing to the inadequate approximation of the initial condition and the influence of the boundary layer, erroneous solutions are obtained at time instances  $t=0, 0.05, 0.1$ .

Fig. 5 illustrates the performance in the absence of considering the constraint equation  $\rho = \langle r \rangle$  in the loss function, while ensuring the exact satisfaction of the initial condition. However, it is evident that the solutions at time  $t=0.05, 0.1$  are incorrect. Consequently, we incorporate this constraint into our APNN loss function.

#### Case II. Homogeneous Dirichlet boundary condition with $\varepsilon = 10^{-8}$

Let  $\varepsilon = 10^{-8}$ , boundary condition be  $F_L(v) = F_R(v) = 0$ , and initial condition be

$$f_0(x, v) = g(x) \cdot \frac{3}{\sqrt{2\pi}} e^{-\frac{(3v)^2}{2}}, \quad (3.7)$$

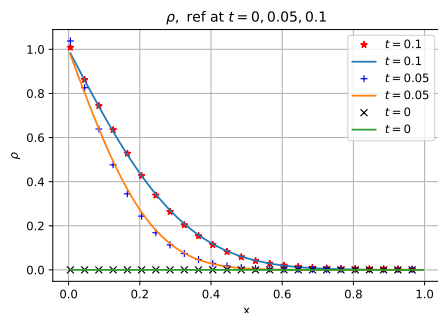


Figure 3: Problem 1—Case I. Plot of density  $\rho$  at  $t=0,0.05,0.1$ : APNNs (marker) vs. Ref (line).  $\varepsilon=10^{-3}$  and neural networks are FCNet with units  $[2,128,128,128,128,1]$  for  $\rho$  and  $[3,256,256,256,256,1]$  both for  $r$  and  $j$ . Batch size is 512 in domain,  $1024 \times 2$  on boundary and 512 on initial.  $\lambda_7=10$  and others are set to be 1. Relative  $\ell^2$  error of APNNs is  $9.87 \times 10^{-3}$ .

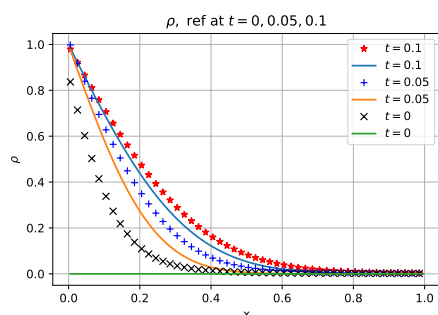


Figure 4: Problem 1—Case I. Plot of density  $\rho$  at  $t=0,0.05,0.1$ : APNNs (marker) vs. Ref (line).  $\varepsilon=10^{-3}$ . And the units of neural networks are  $[2,128,128,128,128,1]$  for  $\rho$  and  $[3,256,256,256,256,1]$  both for  $r$  and  $j$ .

where

$$g(x) = 1 + \sin\left(2\pi x - \frac{\pi}{2}\right). \quad (3.8)$$

Fig. 6 depicts the estimated density, denoted as  $\rho$ , obtained through the utilization of APNNs alongside the reference solution at three distinct time instances, namely  $t=0,0.05,0.1$ . In this particular scenario, it is noteworthy that the function  $f$  exhibits a continuous behavior without any discontinuous jumps, while possessing a non-constant initial value. Evidently, this methodology has proven to yield commendable outcomes, as illustrated in Fig. 6.

**Case III. uncertainty quantification problem with inflow condition** ( $\varepsilon=10^{-5}$ )

Next, we contemplate an uncertainty quantification problem ( $\varepsilon=10^{-5}$ ):

$$\varepsilon \partial_t f + v \partial_x f = \frac{\sigma_S(z)}{\varepsilon} \left( \frac{1}{2} \int_{-1}^1 f dv' - f \right), \quad x_L < x < x_R, \quad -1 \leq v \leq 1, \quad (3.9)$$

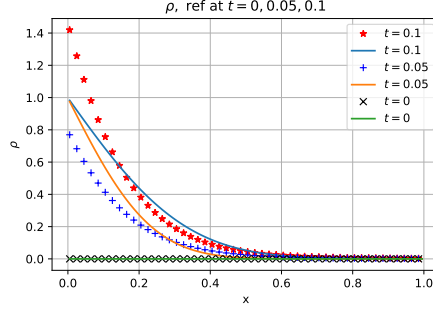


Figure 5: Problem 1—Case I. Plot of density  $\rho$  at  $t=0,0.05,0.1$ : APNNs (marker) vs. Ref (line).  $\varepsilon=10^{-3}$ . And the units of neural networks are  $[2,128,128,128,128,1]$  for  $\rho$  and  $[3,256,256,256,256,1]$  both for  $r$  and  $j$ .

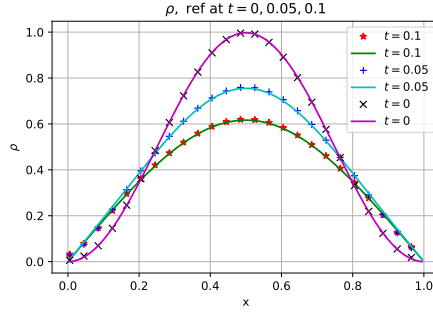


Figure 6: Problem 1—Case II. Plot of density  $\rho$  at  $t=0.05,0.1$ : APNNs (marker) vs. Ref (line).  $\varepsilon=10^{-8}$  and the units of neural networks are  $[2,128,128,128,128,1]$  for  $\rho$  and  $[3,256,256,256,256,1]$  both for  $r$  and  $j$ . Batch size is 1024 in domain,  $512 \times 2$  on boundary and 512 on initial.  $\lambda_3=\lambda_4=\lambda_7=10$  and others are set to be 1. Relative  $\ell^2$  error of APNNs is  $1.25 \times 10^{-2}$ .

with scattering coefficient

$$\sigma_S(\mathbf{z}) = 1 + \frac{1}{10} \prod_{j=1}^{20} \sin(\pi z^j), \mathbf{z} = (z^1, z^2, \dots, z^{20}) \sim \mathcal{U}(\mathcal{Z} = [-1, 1]^{20}), \quad (3.10)$$

and in-flow boundary condition  $F_L(v) = 1, F_R(v) = 0$ , and initial condition  $f_0(x, v) = 0$ .

In order to address this issue, we incorporate the 20-dimensional stochastic vector  $\mathbf{z}$  as a constituent of the input components of the deep neural networks for  $\rho, r, j$ . Similarly, it is possible to derive the empirical APNN risk for the even-odd system of linear transport equation with uncertainties in the following manner

$$\mathcal{R}_{\text{APNN, uq}}^\varepsilon = \mathcal{R}_{\text{residual}}^\varepsilon + \mathcal{R}_{\text{constraint}}^\varepsilon + \mathcal{R}_{\text{initial}}^\varepsilon + \mathcal{R}_{\text{boundary}}^\varepsilon, \quad (3.11)$$



where  $\mathcal{R}_{\text{residual}}^\varepsilon, \mathcal{R}_{\text{constraint}}^\varepsilon, \mathcal{R}_{\text{boundary}}^\varepsilon, \mathcal{R}_{\text{initial}}^\varepsilon$  are denoted by

$$\begin{aligned} \mathcal{R}_{\text{residual}}^\varepsilon &= \frac{\lambda_1}{N_1^{(1)}} \sum_{i=1}^{N_1^{(1)}} |\varepsilon^2 \partial_t r_\theta^{\text{NN}}(\mathbf{z}_i, t_i, x_i, v_i) + \varepsilon^2 v \partial_x j_\theta^{\text{NN}}(\mathbf{z}_i, t_i, x_i, v_i) \\ &\quad - \sigma_S(\mathbf{z}_i) (\rho_\theta^{\text{NN}}(\mathbf{z}_i, t_i, x_i) - r_\theta^{\text{NN}}(\mathbf{z}_i, t_i, x_i, v_i))|^2 \\ &\quad + \frac{\lambda_2}{N_1^{(2)}} \sum_{i=1}^{N_1^{(2)}} |\varepsilon^2 \partial_t j_\theta^{\text{NN}}(\mathbf{z}_i, t_i, x_i, v_i) + v \partial_x r_\theta^{\text{NN}}(\mathbf{z}_i, t_i, x_i, v_i) - (-\sigma_S(\mathbf{z}_i) j_\theta^{\text{NN}}(\mathbf{z}_i, t_i, x_i, v_i))|^2 \\ &\quad + \frac{\lambda_3}{N_1^{(3)}} \sum_{i=1}^{N_1^{(3)}} |\partial_t \rho_\theta^{\text{NN}}(\mathbf{z}_i, t_i, x_i) + \langle v \partial_x j_\theta^{\text{NN}} \rangle(\mathbf{z}_i, t_i, x_i)|^2, \\ \mathcal{R}_{\text{initial}}^\varepsilon &= \frac{\lambda_5}{N_3} \sum_{i=1}^{N_3} |\rho_\theta^{\text{NN}}(\mathbf{z}_i, 0, x_i) - \langle f_0 \rangle(\mathbf{z}_i, x_i)|^2 + \frac{\lambda_6}{N_4} \sum_{i=1}^{N_4} |\mathcal{I}(r_\theta^{\text{NN}} + \varepsilon j_\theta^{\text{NN}})(\mathbf{z}_i, x_i, v_i) - f_0(\mathbf{z}_i, x_i, v_i)|^2, \\ \mathcal{R}_{\text{boundary}}^\varepsilon &= \frac{\lambda_7}{N_5} \sum_{i=1}^{N_5} |\mathcal{B}(r_\theta^{\text{NN}} + \varepsilon j_\theta^{\text{NN}})(\mathbf{z}_i, t_i, x_i, v_i) - F_B(\mathbf{z}_i, t_i, x_i, v_i)|^2. \end{aligned}$$

To assess the numerical performance, we evaluate the value of  $\rho$  at specific time instances, namely  $t = 0, 0.05, 0.1$ . This evaluation is based on computing the expected outcome over  $10^4$  simulation iterations, considering  $\mathbf{z}$  as a vector comprising elements  $z^1, z^2, \dots, z^{20}$ .

Fig. 7 exhibits the anticipated density  $\rho$ , trained using APNNs, alongside the reference solutions at time  $t = 0.05, 0.1$ . The results vividly demonstrate the exceptional capabilities of APNNs when dealing with high-dimensional problems.

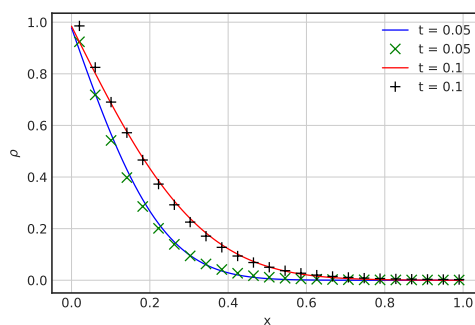


Figure 7: Problem 1—Case III. Plot of density  $\rho$  by taking expectation for  $\mathbf{z}$  at  $t = 0.05, 0.1$  for APNNs (marker) and Ref (line).  $\varepsilon = 10^{-5}, \sigma_S(\mathbf{z}) = 1 + 0.1 \prod_{i=1}^{20} \sin(\pi z_i)$  and the units of neural networks are  $[22, 64, 128, 256, 256, 128, 64, 1]$  for  $\rho$  and  $[23, 128, 256, 512, 512, 256, 128, 1]$  for  $r, j$ . Batch size is 1024 in domain,  $512 \times 2$  for boundary condition and 256 for initial condition.  $\lambda_5 = \lambda_7 = 10$  and others are set to be 1. Relative  $\ell^2$  error of APNNs is  $4.99 \times 10^{-2}$ .

### 3.3 Problem 2: APNNs for solving Boltzmann-BGK equations

Consider the Boltzmann-BGK equation

$$\partial_t f + v \cdot \nabla_x f = \frac{1}{\varepsilon} (M(U) - f), \quad v \in \mathbb{R}. \quad (3.12)$$

and recall the system of BGK model is

$$\begin{cases} \varepsilon(\partial_t f + v \partial_x f) = M(U) - f, \\ \partial_t U + \nabla_x \cdot \langle v m f \rangle = 0, \\ U = \langle m f \rangle. \end{cases}$$

These cases are studied in Problem 2.

**Case I:**  $\varepsilon = 10^{-3}$

$$\begin{aligned} \rho_0(x) &= 1.5 + (0.625 - 1.5) \cdot \frac{\sin(\pi x) + 1}{2}, \\ u_0(x) &= 0, \\ T_0(x) &= 1.5 + (0.75 - 1.5) \cdot \frac{\sin(\pi x) + 1}{2}. \end{aligned}$$

Fig. 8 illustrates the graph representing approximate macroscopic properties at time  $t = 0, 0.1$ . It is evident that the approximate density, momentum, and energy exhibit superior performance compared to those derived from the approximate function  $f$ .

**Case II:**  $\varepsilon = 10^{-3}$

$$\begin{aligned} \rho_0(x) &= 1.5 + (0.625 - 1.5) \cdot \frac{\sin^{\frac{3}{7}}(\pi x) + 1}{2}, \\ u_0(x) &= 0, \\ T_0(x) &= 1.5 + (0.75 - 1.5) \cdot \frac{\sin^{\frac{3}{7}}(\pi x) + 1}{2}. \end{aligned}$$

Fig. 9 illustrates the plot depicting the approximated macroscopic quantities at  $t = 0, 0.1$ . It is noteworthy that the steep slope of  $\rho(0, x)$  and  $T(0, x)$  at  $x = 0$  poses a considerable challenge for obtaining accurate solutions through approximation. The key observation in this scenario is that approximating the moments of  $f$ , namely,  $\rho, u, T$ , is comparatively simpler than approximating  $f$  itself. This assertion holds true across all the test cases.

**Case III:**  $\varepsilon = 10^{-3}$

$$\begin{aligned} \rho_0(x) &= 1.5 + (0.625 - 1.5) \cdot \frac{\tanh(10x) + 1}{2}, \\ u_0(x) &= 0, \\ T_0(x) &= 1.5 + (0.75 - 1.5) \cdot \frac{\tanh(10x) + 1}{2}. \end{aligned}$$

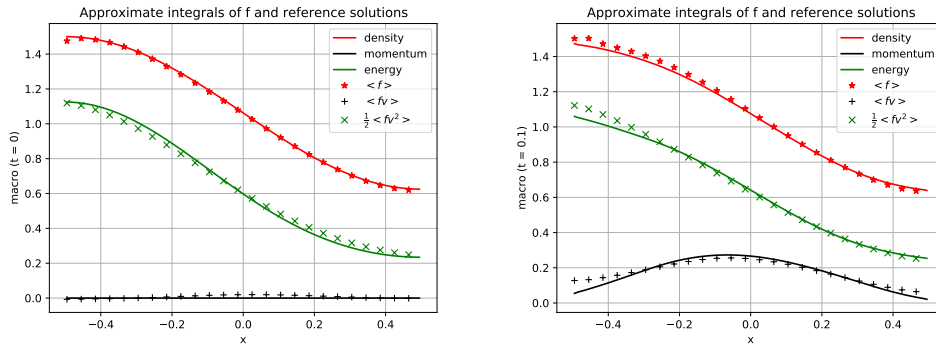
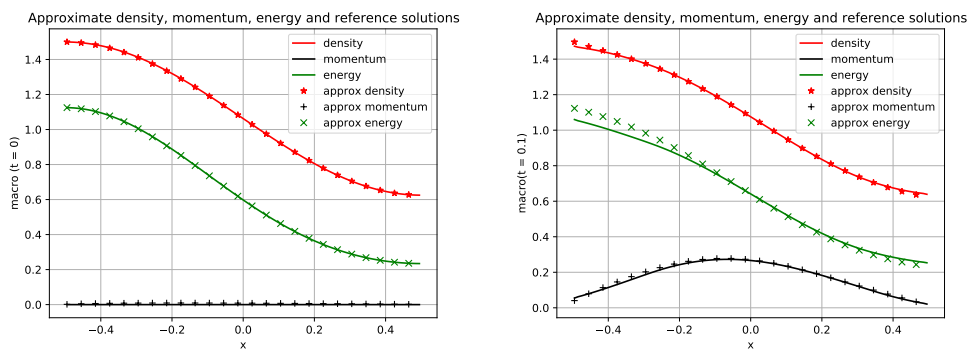
(a) The integrals of approximate  $f$  vs. reference solutions. *Left:  $t=0$  and Right:  $t=0.1$ .*(b) The approximate  $\rho, u, T$  vs. reference solutions. *Left:  $t=0$  and Right:  $t=0.1$ .*

Figure 8: Problem 2—Case I. Plot of density, momentum and energy at time  $t=0,0.1$ : Approximated by APNNs (marker) vs. Ref (line).  $\varepsilon = 10^{-3}$  and the units of neural networks are  $[3,128,128,128,128,128,128,1]$  for  $f$  and  $[2,64,64,64,64,64,64,1]$  both for  $\rho, u$  and  $T$ . Batch size is 512 in domain, and 256 on initial.  $\lambda_5 = (1,10,10), \lambda_6 = 10$  and others are set to be 1. For  $t=0$ : mean square error of density, momentum and energy are  $7.16e-8, 4.50e-6, 8.13e-7$ . For  $t=0.1$ : relative  $l^2$  error of density, momentum and energy are  $5.43e-3, 6.35e-3, 4.47e-2$ .

Fig. 10 depicts the graph illustrating the plot of approximate macroscopic quantities at  $t=0,0.1$ . In this particular scenario, the gradient of  $\rho(0,x)$  and  $T(0,x)$  at  $x=0$  exhibits a seamless behavior. It is evident that the approximate solutions align well with the reference solutions; however, the first moment computed by the approximate function  $f$  yields unsatisfactory outcomes in the vicinity of  $x=0$ . This observation concurs with the findings presented in cases I and II.

**Case IV:**  $\varepsilon = 1$

$$\rho_0(x) = 1.5 + (0.625 - 1.5) \cdot \frac{\tanh(20x) + 1}{2},$$

$$u_0(x) = 0,$$

$$T_0(x) = 1.5 + (0.75 - 1.5) \cdot \frac{\tanh(20x) + 1}{2}.$$

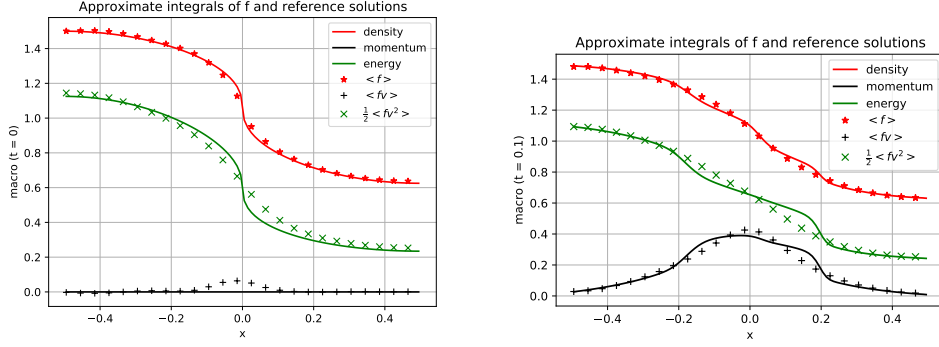
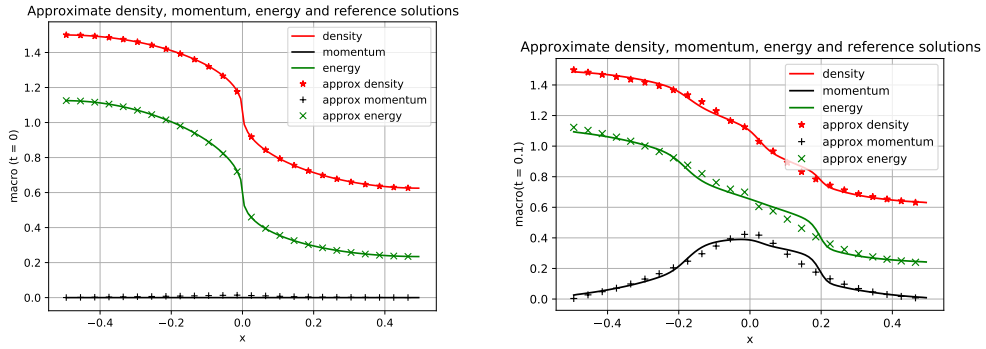
(a) The integrals of approximate  $f$  vs. reference solutions. *Left:  $t=0$  and Right:  $t=0.1$ .*(b) The approximate  $\rho, u, T$  vs. reference solutions. *Left:  $t=0$  and Right:  $t=0.1$ .*

Figure 9: Problem 2—Case II. Plot of density, momentum and energy at time  $t=0,0.1$ : Approximated by APNNs (marker) vs. Ref (line).  $\varepsilon = 10^{-3}$  and the units of neural networks are  $[3,128,128,128,128,128,128,1]$  for  $f$  and  $[2,64,64,64,64,64,64,1]$  both for  $\rho, u$  and  $T$ . Batch size is 512 in domain, and 256 on initial.  $\lambda_5 = (1,10,10)$  and others are set to be 1. For  $t=0$ : mean square error of density, momentum and energy are  $1.29e-4, 6.34e-6, 4.41e-5$ . For  $t=0.1$ : relative  $l^2$  error of density, momentum and energy are  $1.36e-2, 2.00e-2, 3.99e-2$ .

The plot displayed in Fig. 11 illustrates the representation of estimated macroscopic quantities at time instances  $t=0,0.1$ . It is worth noting that this particular scenario closely resembles a realistic problem. In this context, our proposed APNN method demonstrates commendable efficacy by offering favorable solutions when compared to the reference solutions.

Fig. 12 illustrates the relative  $l^2$  discrepancy in density, momentum, and energy throughout the training process. An intriguing observation emerges, wherein the convergence of density and momentum outpaces that of energy across all instances, encompassing  $\varepsilon = 1$  and  $10^{-3}$ . Training the energy component proves notably more challenging.

Table 1 documents the mean square error of risks  $\mathcal{R}_{\text{residual}}^\varepsilon, \mathcal{R}_{\text{claw}}^\varepsilon$ , and  $\mathcal{R}_{\text{constraint}}^\varepsilon$  across these scenarios.

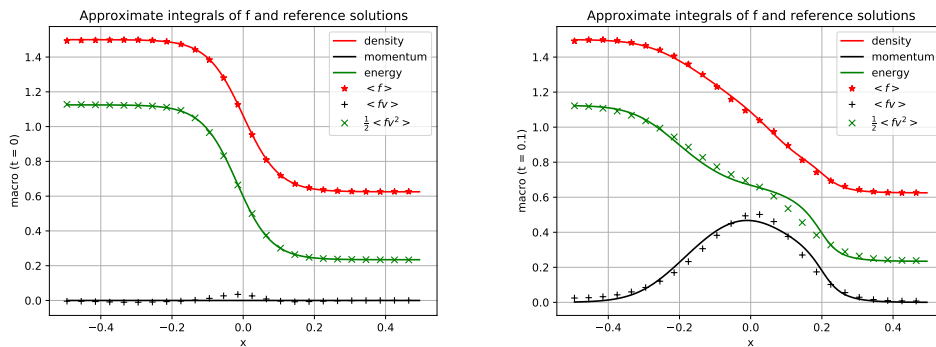
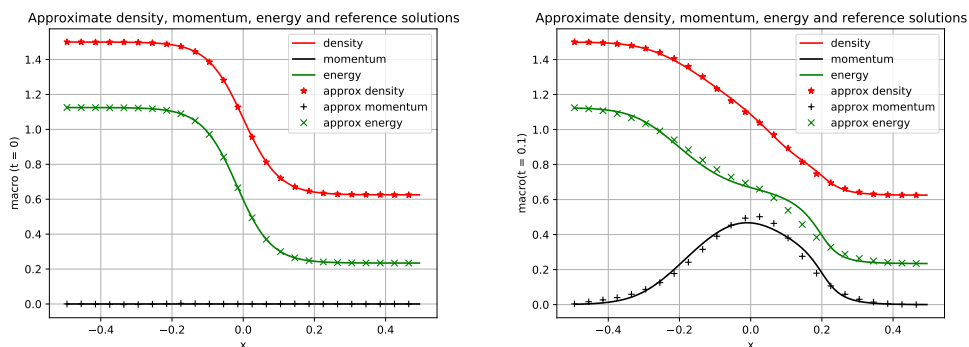
(a) The integrals of approximate  $f$  vs. reference solutions. *Left:  $t=0$  and Right:  $t=0.1$ .*(b) The approximate  $\rho, u, T$  vs. reference solutions. *Left:  $t=0$  and Right:  $t=0.1$ .*

Figure 10: Problem 2—Case III. Plot of density, momentum and energy at time  $t=0,0.1$ : Approximated by APNNs (marker) vs. Ref (line).  $\varepsilon = 10^{-3}$  and the units of neural networks are  $[3, 128, 128, 128, 128, 128, 128, 1]$  for  $f$  and  $[2, 64, 64, 64, 64, 64, 64, 1]$  both for  $\rho, u$  and  $T$ . Batch size is 512 in domain, and 256 on initial.  $\lambda_5 = (1, 10, 10), \lambda_6 = 10$  and others are set to be 1. For  $t=0$ : mean square error of density, momentum and energy are  $4.87e-8, 1.22e-6, 3.29e-8$ . For  $t=0.1$ : relative  $l^2$  error of density, momentum and energy are  $6.19e-3, 1.78e-2, 3.60e-2$ .

**Case V:**  $\varepsilon = 10^{-2}$

$$\rho_0(x) = \begin{cases} 1.5, & x < 0, \\ 0.625x \geq 0, \end{cases}$$

$$u_0(x) = 0,$$

$$T_0(x) = \begin{cases} 1.5, & x < 0, \\ 0.75x \geq 0. \end{cases}$$

The figure depicted in Fig. 13 illustrates the graphical representation of the estimated macroscopic variables at the instant of  $t=0$ .

Fig. 14 depicts the graphical representation of the approximated macroscopic quantities spanning from  $t=0.005$  to  $t=0.05$ . Notably, at  $t=0.005 < \varepsilon$ , a discernible transition in the macroscopic solutions becomes evident.

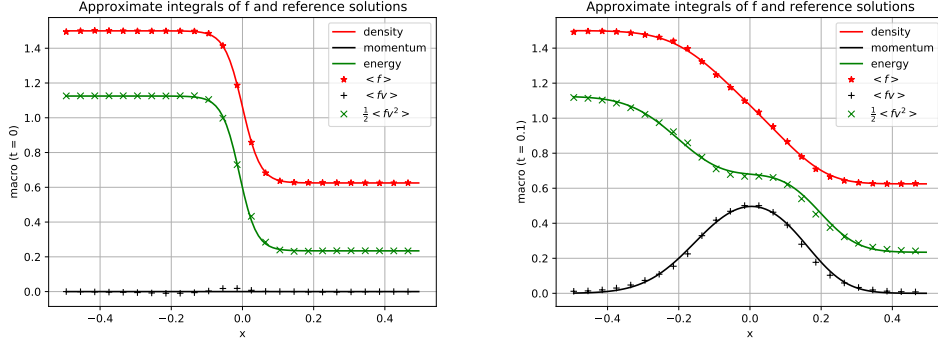
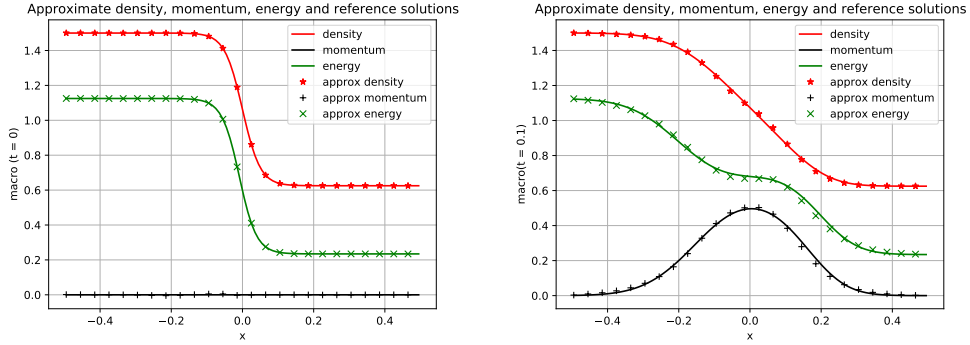
(a) The integrals of approximate  $f$  vs. reference solutions. *Left:  $t=0$  and Right:  $t=0.1$ .*(b) The approximate  $\rho, u, T$  vs. reference solutions. *Left:  $t=0$  and Right:  $t=0.1$ .*

Figure 11: Problem 2—Case IV. Plot of density, momentum and energy at time  $t=0,0.1$ : Approximated by APNNs (marker) vs. Ref (line).  $\varepsilon=1$  and the units of neural networks are  $[3,128,128,128,128,128,1]$  for  $f$  and  $[2,64,64,64,64,64,1]$  both for  $\rho, u$  and  $T$ . Batch size is 512 in domain, and 256 on initial.  $\lambda_5 = (1,10,10), \lambda_6 = 10$  and others are set to be 1. For  $t=0$ : mean square error of density, momentum and energy are  $9.89e-8, 2.34e-6, 2.08e-7$ . For  $t=0.1$ : relative  $l^2$  error of density, momentum and energy are  $6.41e-3, 8.72e-3, 1.62e-2$ .

## 4 Discussion and conclusion

In this paper, we have devised novel and efficient APNNs to numerically address the multiscale kinetic equations involving diffusive scaling. Our APNNs, utilizing parity equations, is employed to solve the linear transport equation. The crucial factor lies in one's concern for physical conservation and the inflow boundary condition. Furthermore, concerning the BGK equation, it is worth noting that the collision operator present on the right-hand side exhibits both nonlinearity and non-locality, along with a boundary layer effect. In order to address this, we have devised an APNN method that precisely enforces the boundary conditions. The most noteworthy observation derived from this study is that approximating the zeroth, first, and second moments of the particle's density distribution is comparatively easier than approximating the distribution

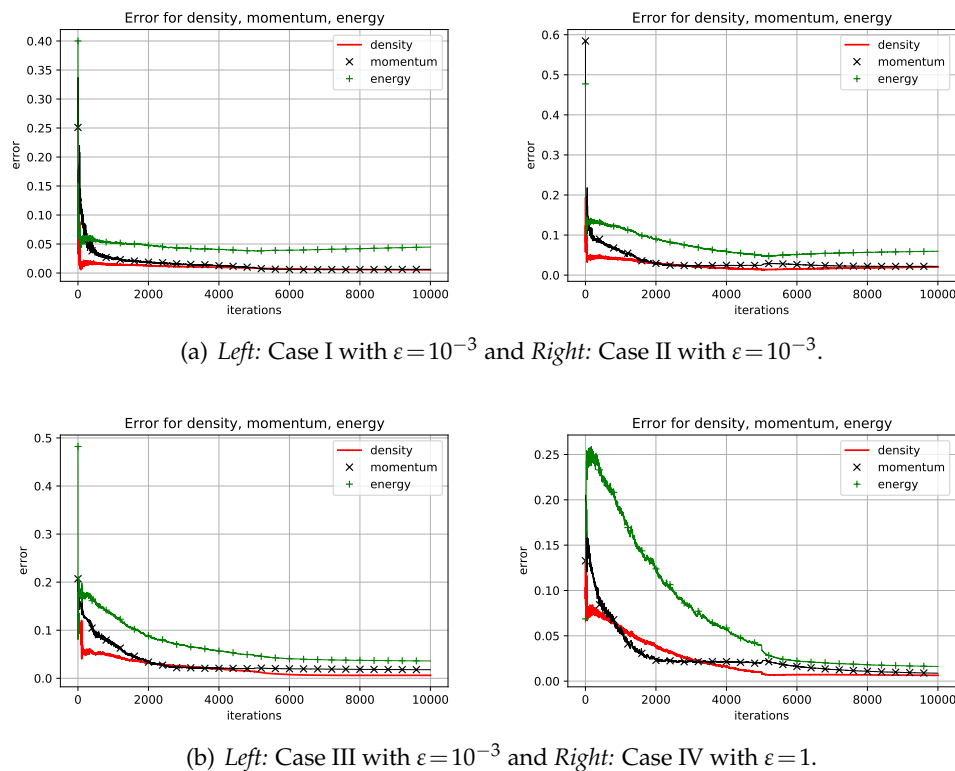


Figure 12: Problem 2. Plot of the change of error for density, momentum and energy approximated by APNNs.

itself. During the training process, a phenomenon becomes apparent: the convergence of momentum and energy is slower in comparison to that of density. This discrepancy is likely influenced by the value of  $\varepsilon$ . The question that arises is how to explain this phenomenon. In addition to the above, the construction of the neural network holds tremendous significance when dealing with the multiscale equations.

## Acknowledgement

### References

- [1] François Bouchut, François Golse, and Mario Pulvirenti. Kinetic equations and asymptotic theory. Elsevier, 2000.
- [2] Giacomo Dimarco and Lorenzo Pareschi, Numerical methods for kinetic equations. Acta Numerica, 23:369-520, 2014.
- [3] Shi Jin. Asymptotic preserving (AP) schemes for multiscale kinetic and hyperbolic equations: a review. Lecture notes for summer school on methods and models of kinetic theory (M&MKT), Porto Ercole (Grosseto, Italy), pages 177-216, 2010.
- [4] Weinan E. Principles of multiscale modeling. Cambridge University Press, 2011.

Table 1: Mean square errors of risks  $\mathcal{R}_{\text{residual}}^\varepsilon$ ,  $\mathcal{R}_{\text{claw}}^\varepsilon$  and  $\mathcal{R}_{\text{constraint}}^\varepsilon$  in terms of four cases.

Case	Risk	$\mathcal{R}_{\text{residual}}^\varepsilon$	$\mathcal{R}_{\text{claw}}^\varepsilon$			$\mathcal{R}_{\text{constraint}}^\varepsilon$		
			density	momentum	energy	0-order	1-order	2-order
I		3.92e-6	7.01e-7	1.70e-5	6.42e-7	1.80e-6	1.77e-5	8.17e-7
II		1.30e-5	1.16e-5	1.97e-5	9.58e-6	1.67e-5	4.20e-5	1.63e-5
III		1.54e-5	1.81e-6	4.67e-6	3.73e-6	1.95e-6	1.61e-5	8.20e-7
IV		6.24e-5	5.90e-6	1.30e-5	2.09e-5	3.62e-6	6.08e-6	5.07e-6

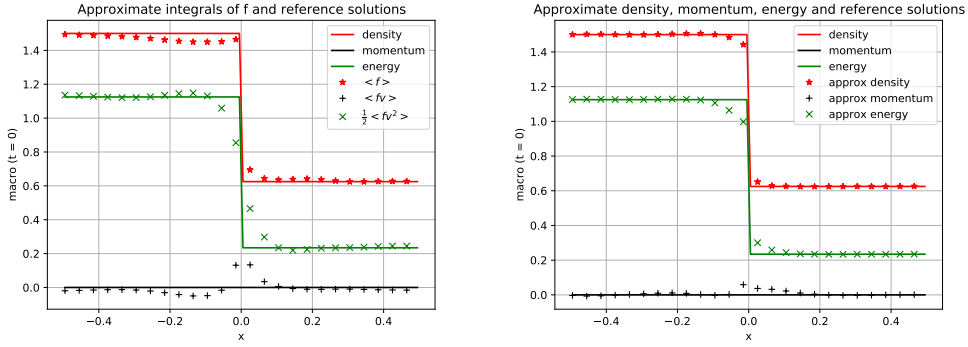


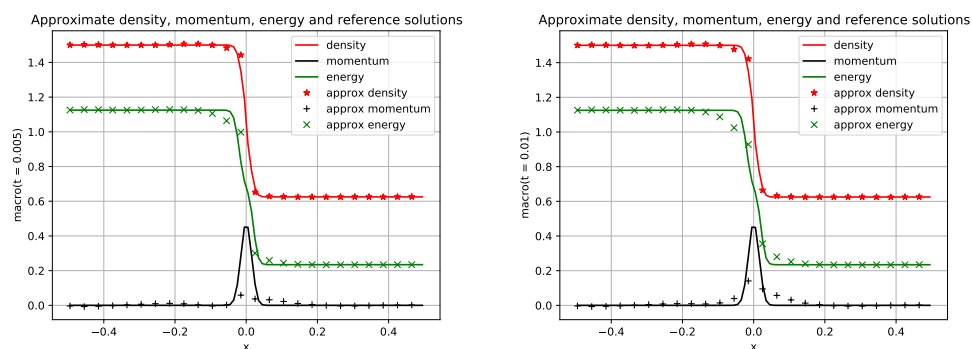
Figure 13: Problem 2—Case V. Plot of density, momentum and energy at time  $t=0$ : Approximated by APNNs (marker) vs. Ref (line).  $\varepsilon=10^{-2}$  and the units of neural networks are  $[3,128,128,128,128,128,128,1]$  for  $f$  and  $[2,96,96,96,96,96,96,1]$  both for  $\rho, u$  and  $T$ . Batch size is 512 in domain, and 512 on initial.  $\lambda_3=(10,10,1), \lambda_5=(1,100,100), \lambda_6=100$  and others are set to be 1.

- [5] Christian Beck, Martin Hutzenthaler, Arnulf Jentzen, and Benno Kuckuck. An overview on deep learning-based approximation methods for partial differential equations, arXiv preprint arXiv:2012.12348, 2020.
- [6] Zhiqiang Cai, Jingshuang Chen, and Min Liu. Least-squares relu neural network (lsnn) method for linear advection-reaction equation. *Journal of Computational Physics*, page 110514, 2021.
- [7] Weinan E and Bing Yu. The deep ritz method: A deep learning-based numerical algorithm for solving variational problems. *Communications in Mathematics and Statistics*, 6(1):1–12, 2018.
- [8] Yulei Liao and Pingbing Ming. Deep nitsche method: Deep ritz method with essential boundary conditions. *Communications in Computational Physics*, 29(5):1365–1384, 2021.
- [9] Liyao Lyu, Zhen Zhang, Minxin Chen, and Jingrun Chen. Mim: A deep mixed residual method for solving high-order partial differential equations. *Journal of Computational Physics*, 452:110930, 2022.
- [10] Maziar Raissi, Paris Perdikaris and George E Karniadakis. Physics-informed neural networks: A deep learning framework for solving forward and inverse problems involving nonlinear partial differential equations. *Journal of Computational Physics*, 378:686–707, 2019.
- [11] Justin Sirignano and Konstantinos Spiliopoulos. DGM: A deep learning algorithm for solving partial differential equations. *Journal of Computational Physics*, 375:1339–1364, 2018.

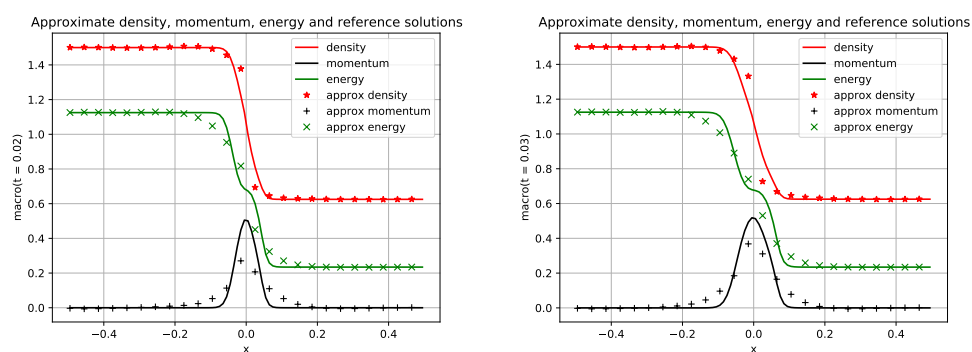


- [12] Yaohua Zang, Gang Bao, Xiaojing Ye, and Haomin Zhou. Weak adversarial networks for high-dimensional partial differential equations. *Journal of Computational Physics*, page 109409, 2020.
- [13] Zongyi Li, Nikola Borislavov Kovachki, Kamyar Azizzadenesheli, Burigede liu, Kaushik Bhattacharya, Andrew Stuart, and Anima Anandkumar. Fourier neural operator for parametric partial differential equations. In *International Conference on Learning Representations*, 2021.
- [14] Lu Lu, Pengzhan Jin, Guofei Pang, Zhongqiang Zhang, and George Em Karniadakis. Learning nonlinear operators via deeponet based on the universal approximation theorem of operators. *Nature Machine Intelligence*, 3(3):218–229, 2021.
- [15] Lulu Zhang, Tao Luo, Yaoyu Zhang, Weinan E, Zhi-Qin John, and Zheng Ma. Mod-net: A machine learning approach via model-operator-data network for solving pdes. *Communications in Computational Physics*, 32(2):299–335, 2022.
- [16] Zongyi Li, Hongkai Zheng, Nikola Kovachki, David Jin, Haoxuan Chen, Burigede Liu, Kamyar Azizzadenesheli, and Anima Anandkumar. Physics-informed neural operator for learning partial differential equations. *arXiv preprint arXiv:2111.03794*, 2021.
- [17] Sifan Wang, Hanwen Wang, and Paris Perdikaris. Learning the solution operator of parametric partial differential equations with physics-informed deeponets. *Science advances*, 7(40):eabi8605, 2021.
- [18] Wei Xiong, Xiaomeng Huang, Ziyang Zhang, Ruixuan Deng, Pei Sun, and Yang Tian. Koopman neural operator as a mesh-free solver of non-linear partial differential equations. *arXiv preprint arXiv:2301.10022*, 2023.
- [19] Zheng Chen, Liu Liu, and Lin Mu. Solving the linear transport equation by a deep neural network approach. *Discrete and Continuous Dynamical Systems - S*, 15(4):669–686, 2022.
- [20] Hyung Ju Hwang, Jin Woo Jang, Hyeontae Jo, and Jae Yong Lee. Trend to equilibrium for the kinetic fokker-planck equation via the neural network approach. *Journal of Computational Physics*, 419:109665, 2020.
- [21] Shi Jin, Zheng Ma, and Keke Wu. Asymptotic-preserving neural networks for multiscale time-dependent linear transport equations. *Journal of Scientific Computing*, 94(3):57, 2023.
- [22] Yulong Lu, Li Wang, and Wuzhe Xu. Solving multiscale steady radiative transfer equation using neural networks with uniform stability. *Research in the Mathematical Sciences*, 9(3):1–29, 2022.
- [23] Hongyan Li, Song Jiang, Wenjun Sun, Liwei Xu, and Guanyu Zhou. A model-data asymptotic-preserving neural network method based on micro-macro decomposition for gray radiative transfer equations. *arXiv preprint arXiv:2212.05523*, 2022.
- [24] Giulia Bertaglia. Asymptotic-preserving neural networks for hyperbolic systems with diffusive scaling. In *Advances in Numerical Methods for Hyperbolic Balance Laws and Related Problems*, pages 23–48. Springer Nature Switzerland, 2023.
- [25] Giulia Bertaglia, Chuan Lu, Lorenzo Pareschi, and Xueyu Zhu. Asymptotic-preserving neural networks for multiscale hyperbolic models of epidemic spread. *Mathematical Models and Methods in Applied Sciences*, 32(10):1949–1985, 2022.
- [26] Qin Lou, Xuhui Meng, and George Em Karniadakis. Physics-informed neural networks for solving forward and inverse flow problems via the boltzmann-bgk formulation. *Journal of Computational Physics*, 447:110676, 2021.
- [27] Kaiming He, Xiangyu Zhang, Shaoqing Ren, and Jian Sun. Deep residual learning for image recognition. In *Proceedings of the IEEE conference on computer vision and pattern recognition*, pages 770–778, 2016.
- [28] Carlo Cercignani. *Rarefied gas dynamics: from basic concepts to actual calculations*, volume 21. Cambridge university press, 2000.

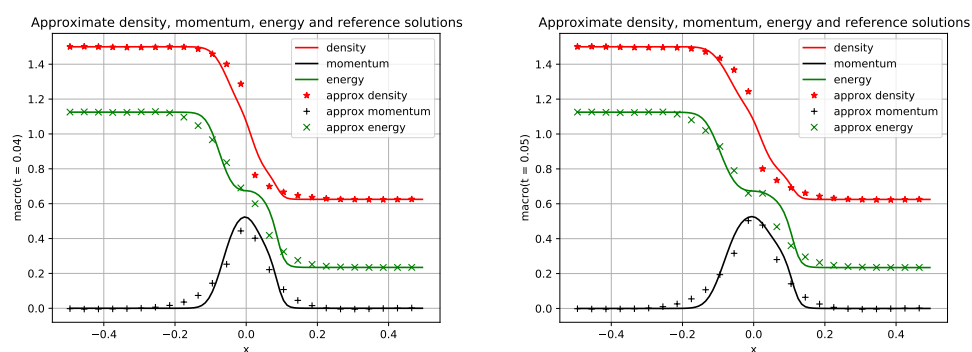
- [29] Maurice N Kogan. Rarefied gas dynamics. Springer, 2013.
- [30] Mounir Bennoune, Mohammed Lemou, and Luc Mieussens. Uniformly stable numerical schemes for the boltzmann equation preserving the compressible navier–stokes asymptotics. *Journal of Computational Physics*, 227(8):3781–3803, 2008
- [31] Francois Coron and Benoit Perthame. Numerical passage from kinetic to fluid equations. *SIAM Journal on Numerical Analysis*, 28(1):26–42, 1991.
- [32] P Bhathnagar, E Gross, and Max Krook. A model for collision processes in gases. *Physical Review*, 94(3):511, 1954.
- [33] Kun Xu. A gas-kinetic bgk scheme for the navier–stokes equations and its connection with artificial dissipation and godunov method. *Journal of Computational Physics*, 171(1):289–335, 2001.
- [34] Hua-Zhong Tang. Gas-kinetic schemes for compressible flow of real gases. *Computers & Mathematics with Applications*, 41(5-6):723–734, 2001.
- [35] Diederik P Kingma and Jimmy Ba. Adam: A method for stochastic optimization. In *ICLR*, 2015.
- [36] Lu Lu, Xuhui Meng, Zhiping Mao, and George Em Karniadakis. Deepxde: A deep learning library for solving differential equations. *SIAM Review*, 63(1):208–228, 2021.



(a) The approximate  $\rho, u, T$  vs. reference solutions. *Left:*  $t = 0.005$  and *Right:*  $t = 0.01$ .



(b) The approximate  $\rho, u, T$  vs. reference solutions. *Left:*  $t = 0.02$  and *Right:*  $t = 0.03$ .



(c) The approximate  $\rho, u, T$  vs. reference solutions. *Left:*  $t = 0.04$  and *Right:*  $t = 0.05$ .

Figure 14: Plot of density, momentum and energy at time  $t = 0.005$  to  $0.05$ : Approximated by APNNs (marker) vs. Ref (line).